MRS Communications (2020), 1 of 10

doi:10.1557/mrc.2020.39

MRS Communications

Research Letter

Light angle dependence of photothermal properties in oxide and porphyrin thin films for energy-efficient window applications

Mengyao Lyu and **Jou Lin,** The Materials Science and Engineering Program, Department of Mechanical and Materials Engineering, College of Engineering and Applied Science, University of Cincinnati, Cincinnati, OH 45221, USA
John Krupczak Jr., Department of Engineering, Hope College, Holland, MI 49423, USA
Donglu Shi, The Materials Science and Engineering Program, Department of Mechanical and Materials Engineering, College of Engineering and Applied Science, University of Cincinnati, Cincinnati, OH 45221, USA

Address all correspondence to Donglu Shi at **shid@ucmail.uc.edu**

(Received 10 April 2020; accepted 26 May 2020)

Abstract

The photothermal experiments on the incident light angle dependence are carried out using simulated solar light on thin films of both iron oxides (Fe_3O_4 and $Fe_3O_4@Cu_{2-x}S$) and porphyrin compounds (chlorophyll and chlorophyllin). Fe_3O_4 and $Fe_3O_4@Cu_{2-x}S$ are synthesized using various solution methods that produce mono-dispersed nanoparticles on the order of 10 nm. Chlorophyll is extracted from fresh spinach and chlorophyllin sodium copper is a commercial product. These photothermal (PT) materials are dispersed in polymethyl methacrylate (PMMA) solutions and deposited on glass substrates via spin coating that result in clear and transparent thin films. The iron-oxide based thin films show distinctive absorption spectra; Fe_3O_4 exhibits a strong peak near UV and gradually decreases into the visible and NIR regions; the absorption of $Fe_3O_4@Cu_{2-x}S$ is similar in the UV region but shows a broad absorption in the NIR region. Both chlorophyll and chlorophyllin are characterized with absorption peaks near UV and NIR showing a "U"-shaped spectrum, ideally required for efficient solar harvest and high transparency in energy-efficient single-pane window applications. Upon coating of the transparent PT films on the window inner surfaces, solar irradiation induces the photothermal effect, consequently raising the film temperature. In this fashion, the thermal loss through the window can be significantly lowered by reducing the temperature difference between the window inner surface and the room interior, based on a new concept of so-called optical thermal insulation (OTI) without any intervention medium, such as air/argon, as required in the glazing technologies. Single-panes are therefore possible to replace double- or triple panes. As OTI is inevitably affected by seasonal and daily sunlight changes, an incident light angle dependence of the photothermal effect is crucial in both thin film and window designs. It is found that the heating curves reach their maxima at small angles of incidence while the photothermal effect is considerably reduced at large angles. This angle dependence is well explained by light reflection by the thin film surface, however, deviated from what is predicted by the Fresnel's law, attributable to non-ideal surfaces of the substrates. The angle dependence data provide an important reference for OTI that window exposure to the sun is greater at winter solstice while that is considerably reduced in the summer. This conclusion indicates much enhanced solar harvesting and heat conversion via optically insulated windows in the winter season, resulting in much lower *U*-factors.

Introduction

A major global change is the rapid sprawling of megacities that present enormous social and environmental challenges. These population-concentrated civic structures not only consume tremendous energy but also exert a huge impact on a sustainable habitat. Conventional buildings are commonly structured with windows enframed within the building walls that compromise between lighting and heat transfer. The recent technological advancement has enabled glass-based building facades with double- or triple-glazed transparent panels. However, the conventional glazing technologies cannot effectively control thermal energy loss and gain, be it conductive or radiative. The residential and commercial buildings account for about 40% (or about 40 quadrillion British thermal units) of the total U.S. energy consumption.[1]

As is well known, photons can be absorbed by spectral-selective materials and converted to other forms of energy such as heat and electricity.[2–4] Those that are photonically activated to create heat are categorized as the photothermal (PT) materials, and the photovoltaics (PV) are characterized by the ability to convert photons to electricity. The common characteristics of these materials are the photon-to-heat/electricity conversion efficiencies that vary depending primarily on the absorption spectra of the materials. While photovoltaic solar cells have been widely applied for clean and alternative energy, photothermal materials are recently beginning to gain tremendous interest in the energy industry. Another very important feature of novel PT and PV materials is high transparency for visible light. This unique property requires the thin film to be not only highly absorbent in the UV and NIR regions for efficient solar light harvesting but also transparent in the visible band for a variety of applications, one of which is in making energy-efficient single-pane windows.[5–9]

Optical thermal insulation (OTI) has been recently proposed and implemented without any intervening medium based on photothermal materials.[10] OTI does not rely on any conventional thermal insulating materials or gases, such as air or argon, as often used in conventional double-pane windows, but achieves its effectiveness via photothermally heated building skins. If a spectral-selective thin film is applied on a window inner surface that exhibits strong UV/NIR absorptions and high visible transmittance, the pronounced photothermal (PT) effect will be photonically activated to increase the surface temperature.[11] Under solar irradiation, the inner surface of window will be heated to reduce the temperature difference, ΔT, between the single-pane (without glazing) and the room interior. This reduction in ΔT will effectively lower heat transfer through the building skin, characterized by a low *U*-factor, therefore achieving the goal of energy saving without double- or triple-glazing.[12] The PT materials identified in this study are abundant in nature and environmentally friendly. If successful, this novel approach will transform the current civic structures by creating an energy harvesting building skin that efficiently utilizes solar irradiation in a spectrally selective fashion.

Heat loss through windows is characterized by the so-called *U*-factor that literally translates to thermal transmittance. *U*-factor is defined as the ratio of the heat flux *H* per unit area through the pane to the difference ΔT between the interior and exterior temperatures.[13] A lower *U*-factor indicates a higher thermal insulation or lower energy transfer through a window. The *U*-factor for an entire window, which includes the effects of the sash and the framing around the windowpane, needs to be less than 1.7 $W/m^2 \cdot K$ (0.30 $Btu/h \cdot ft^2 \cdot {}^\circ F$) in order to satisfy the Energy Star certification in the U.S. colder regions.[14] This criterion of *U*-factor has been conventionally achieved by using double- or triple panes. Under extremely cold conditions, the temperature of the interior surface of a single-pane window is nearly as low as the outside temperature, which causes a significant heat loss. The current technology for efficient windows relies upon the double-pane or even triple-pane insulated glass unit with a low-emissivity (low-e) coating. Since only a few transparent and insulation materials that are economically available, OTI has been shown very effective for window applications with satisfying *U*-factors.[10,15]

Despite significant thermal loss reduction by OTI, another critical issue deals with seasonal factors that can significantly compromise the overall energy consumptions through windows. One of the major requirements of OTI is the strong absorption of solar light in the UV and NIR regions. The surface photothermal heating can be affected by both angle of incidence[16,17] and reflectivity of the surface.[18] For instance, the reflectance of light is at the minimum when the incident light is normal to the plane of the interface ($\theta = 0°$), while that is significantly increased at a large angle of incidence ($\theta \sim 90°$) according to Fresnel's law.[19] Therefore, the photothermal effect will inevitably vary depending up how much light is being absorbed or reflected by the PT thin film. For window applications, we define the direct angle, α, at which the sun rays strike the ground.

For seasonal and daily changes on earth that control the incident angle of the sun, we consider a cold region in northern America, Chicago, with a north latitude of 41.8° at winter solstice. When sunlight is directed perpendicular to a given line of longitude, the time of the day is considered Solar Noon.[20,21] Under these conditions, the incident angle of the sun, α, can be determined by the equation: $\alpha = 90°$-[latitude (φ)−earth tilt angle (δ)] [Fig. 1(a)].[22] At the winter solstice, the sun is south of the equator, $\delta = -23.5°$. We then have $\alpha = 24.70°$. This low angle of α provides more sun-exposed area of the window as illustrated in Fig. 1(b). At the summer solstice, $\delta = 23.5°$, $\alpha = 71.70°$, resulting in less sun rays through the windows [Fig. 1(c)]. The results of the above calculations indicate the seasonal effects of the sunlight incident angles on the photothermal heating at window surfaces, especially when considering the difference between the winter and summer solstice. During the winter season, more pronounced photothermal effect is required/desired in order to reduce heat loss through the window surfaces, a condition in fact favored by a small α [Fig. 1(b)]. In contrast, the photothermal effect should be minimized for undesirable heating in the summer, which is naturally reduced by a large α [Fig. 1(c)].

In this study, we investigated the effects of the light incident angle, θ, on the photothermal heating for several PT thin films including Fe_3O_4, $Fe_3O_4@Cu_{2-x}S$, chlorophyll, and chlorophyllin using a solar-simulated light source. The PT thin films were synthesized following the previously reported methods but modified on optimum concentrations and microstructures. These thin films were deposited on glass substrates and their photothermal and optical properties were characterized and optimized for single-pane applications.

Experiment details

Materials synthesis

The chemicals of this research including iron (III) acetylacetonate [$Fe(acac)_3$, ≥99.9%], copper(II) acetylacetonate [$Cu(acac)_2$, ≥99.9%], oleylamine (70%), sulfur (99.998%), *N*-methyl-2-pyrrolidone (99.5%), and chloroform (≥99.9%) were purchased from Sigma-Aldrich Inc. Cyclohexane was purchased from Tedia Inc. Poly (methyl methacrylate) was purchased from Polysciences.

Fe_3O_4 and $Fe_3O_4@Cu_{2-x}S$ nanoparticles were synthesized by a modified procedure from the literature.[10] Specifically, 90 mL oleylamine was heated to 300 °C in a three-necked flask and stirred for 30 min in nitrogen environment. A solution containing 18 mL oleylamine, 12 mL *N*-methyl-2-pyrrolidone, and 1.59 g $Fe(acac)_3$ was injected into the flask. After keeping at 300 °C for 10 min, it was cooled to 60 °C for 10 min. At room temperature, the nanoparticles were collected by centrifugation and washed twice with methanol. The collected

https://doi.org/10.1557/mrc.2020.39

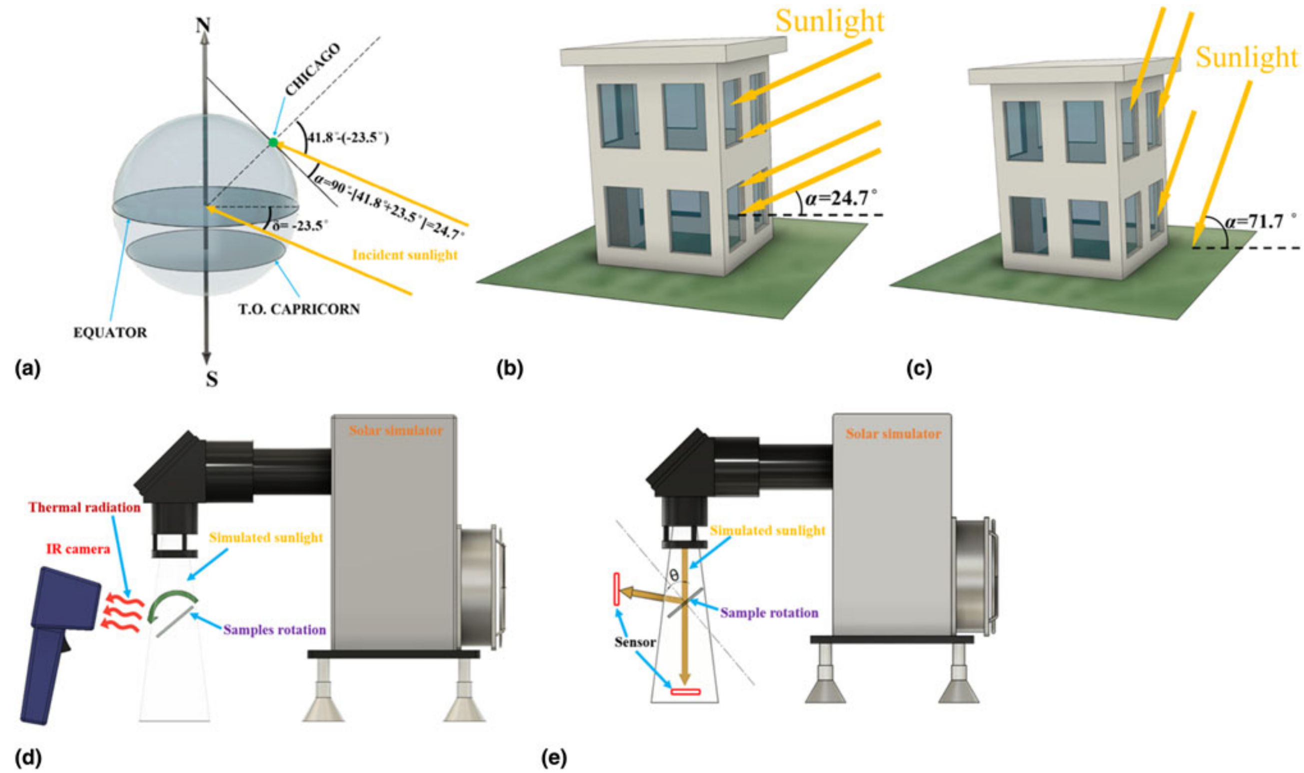

Figure 1. Schematic diagrams of (a) the incident sunlight angle α in the winter season of Chicago, (b) low sunlight incident angle of α for more sun-exposed area on window surfaces in winter, (c) high sunlight incident angle of α for less sun-exposed area on window surfaces in winter, (d) angle dependence measurement set up, (e) reflectance and transmittance measurements.

nanoparticles were freeze-dried using a Labconco freeze dryer. After drying, the Fe_3O_4 nanoparticles were dispersed in toluene for later use. The Fe_3O_4@$Cu_{2-x}S$ nanoparticles were synthesized by a procedure similar to the synthesis of the Fe_3O_4 nanoparticles. The solution was kept at 300 °C for 10 min, then slowly cooled to 70 °C for 10 min. A total of 192 mg of sulfur was dissolved in 18 mL oleylamine, mixed with 15 mL cyclohexane and injected into the previous solution. After stirring at 70 °C for 10 min, 785 mg $Cu(acac)_2$ dissolved in 6 mL oleylamine into which a 24 mL chloroform solution was injected. The final product was kept at 70 °C for 30 min. The Fe_3O_4@$Cu_{2-x}S$ nanoparticles were collected by centrifugation and washed twice with methanol. Upon freeze drying, nanoparticles were dispersed in toluene.

Chlorophyll was extracted from spinach based on a method previously reported.[9] Specifically, a bunch of fresh local spinach leaves was sectioned into small pieces, then freeze-dried at −53 °C for 48 h. The dried leaves (about 5 g) were washed twice using petroleum ether (boiling point 40–60 °C) to remove the carotenoids and waxes. The washed leaves were immersed and stirred in 200 mL of methanol/petroleum ether mixture with 3:1 volume ratio at room temperature overnight. The remaining solid substance was removed by filtration and the solution was transferred to a separatory funnel, then washed twice by using 200 mL NaCl solution. The organic phase was removed by filtration and rotary evaporation. The isolated film was dissolved in 50 mL of acetone and stored at −20 °C for 24 h to precipitate impurities. Precipitates were deposited by centrifugation and the supernatant was collected. Acetone was removed by rotary evaporation. The extracted chlorophyll was dissolved in toluene and stored at −20 °C for future usage. Chlorophyllin sodium copper was purchased from Sigma-Aldrich (St. Louis, MO, US).

Thin film deposition

Fe_3O_4 and Fe_3O_4@$Cu_{2-x}S$ nanoparticles were dispersed in 10 wt% PMMA (polymethyl methacrylate)/toluene solution. The chlorophyll-based thin films were prepared by dissolving chlorophyll into 10 wt%. PMMA/toluene solution. Chlorophyllin was dissolved in 10 wt% PAA (polyacrylic acid)/DI water solution. To prepare the thin film samples, 2.54×2.54 cm^2 micro slides were sonicated in acetone for 15 min, subsequently sonicated in IPA for another 15 min, and dried at 50 °C for 30 min in an Isotemp 500 series oven (Fisher Scientific, Piscataway, New Jersey, US). Thin films were deposited on glass slides by spin coating. A 500 µL nano particle solution was dropped on a 2.54×2.54 cm^2 glass slide at spinning speed of 1000 rpm.

Optical and photothermal property characterization

The absorption and transmittance spectra of the thin films were obtained by using the UV-VIS-NIR spectrometer Lambda 900 (Perkin-Elmer Inc., Waltham, MA). The average visible transmittance (AVT) was measured by a light transmittance meter (LS116, Linshang, Co. Ltd., Shenzhen city, Guangdong province, China).

For photothermal experiments, samples were irradiated by 0.4 W/cm^2 white light using a Newport 150 W solar simulator (Lamp model 67005). The temperature was measured and recorded by using an infrared camera (FLIR E6). The power density of solar simulator was calibrated by an optical power meter (Coherent Inc.). There were two main steps in this experiment, namely, heating and cooling.

The light power density registered on the samples surfaces from the solar simulator is 0.4 W/cm^2. An infrared camera was used to measure the temperature of the samples. For heating curves, temperature was recorded every minute for the first 20 min. After 20 min, the light source was turned off. And the cooling curve was obtained by recording the temperature for 15 min.

Incident light angle dependence measurement

The incident light angle (θ) dependence experimental set up is schematically illustrated in Figs. 1(d) and 1(e). As shown in Fig. 1(d), the simulated solar light is generated by the solar generator (0.4 W/cm^2) and directed from top down. The sample below the light source can be rotated from $\theta = 0°$ to 90° with the coated photothermal film surface facing directly to the solar-simulated light while the photothermal curves are recorded at a given angle. The position of the infrared camera is also shown in Fig. 1(d) that measures the film surface temperature as a function of time (heating curves).

A light power density meter was used to register the light reflectance and transmittance [Fig. 1(e)]. As expected, the reflected light should increase with the increasing angle of incidence, α, that will reach the maximum when the light is near parallel to the film surface.[23,24] The transmitted light is just opposite to the reflected light and it is maximized at $\alpha = 0$, indicating that more photons pass through the thin film sample vertically generating the highest photothermal effect. Therefore, both reflectance and transmittance can be directly correlated to the heating curves.[25,26]

Experimental results

Transmission electron microscopy (TEM) images were taken by using CM-20 TEM [Figs. 2(a) and 2(b)]. As shown in Fig. 3, the average diameter of Fe_3O_4 nanoparticles is around 10 nm [Fig. 2(a)] while that of Fe_3O_4@$Cu_{2-x}S$ about 20 nm [Fig. 2(b)]. As reported previously, both Fe_3O_4 and Fe_3O_4@$Cu_{2-x}S$ nanoparticles can be well dispersed in the PMMA solutions.[27–30]

The scanning electron microscopy (SEM) was carried out by using the SCIOS Dual-Beam SEM/Focused Ion Beam. Figures 2(c)–2(f) show the cross-sections of various samples as indicated. As shown in Figs. 2(c)–2(f), all thin films exhibit rather smooth surfaces but with varied thickness. Both Fe_3O_4 and chlorophyll films share similar thicknesses, respectively, 857 and 836 nm. Fe_3O_4@$Cu_{2-x}S$ (607 nm) and chlorophyllin (481 nm) films are relatively thinner resulting from various processing parameters such as viscosity and concentration.[31] The surfaces and cross-sections of the thin films played crucial roles in both optical and photothermal properties, which were optimized by controlling the amount of solution and rpm of spin coater.[32–34]

Figures 3(a) and 3(b) show optical absorption and transmittance spectra of the Fe_3O_4, Fe_3O_4@$Cu_{2-x}S$, chlorophyll, and chlorophyllin thin films. As shown in Fig. 3(a), the Fe_3O_4 thin film exhibits strong absorption near the UV region and rapidly decrease in the visible region. Only weak absorption is observed in the NIR region. Correspondingly, as shown in Fig. 3(b), the films retain considerable transmittance in the visible region, giving significant transparency. Quite different absorption and transmittance spectra were observed for the Fe_3O_4@$Cu_{2-x}S$ thin film as shown in Figs. 3(a) and 3(b). As shown in Fig. 3(a), the Fe_3O_4@$Cu_{2-x}S$ thin film shows considerable absorption in a wide range of NIR extending up to 1400 nm which is in contrast with that of $Cu_{2-x}S$. This is an important reason for the addition of $Cu_{2-x}S$ to Fe_3O_4 (formation of Fe_3O_4@$Cu_{2-x}S$) for enhanced NIR absorption. Comparable transmittance is observed for the Fe_3O_4@$Cu_{2-x}S$ thin film as shown in Fig. 3(b). The absorptions of both chlorophyll and chlorophyllin thin films exhibit peaks near the UV and NIR regions but much more pronounced in chlorophyllin [Fig. 3 (a)]. Note that there is considerable noise between 800 and 1000 nm due to switching of slit at around 900 nm. As shown in Fig. 3(a), the absorption peaks of chlorophyll are at about 409 and 667 nm, while those of chlorophyllin around 407 and 632 nm.[35–37] These optical features are particularly important for window applications: highly absorbent in the UV and NIR regions for efficient solar harvesting and conversion, while remaining transparent, i.e., low absorption in the visible region, characterized by the "Saddle-like" shape.[9]

The absorption coefficient (α) can be expressed as[38]: $\alpha = \alpha_o \exp[\sigma(E - E\mathrm{o})/K_BT]$, where α_o is an absorption-related constant, E is the incident energy, E_o is the onset of absorption, and $E_u = K_BT/\sigma$ is Urbach energy[39], where σ is the steepness parameter and K_B is the Boltzmann constant. Urbach energy is a measure of defect density in the crystal. Both α_o and E_o are material-dependent constants. Based on this relationship, the direct band gap value of the material can be estimated by plotting $(E\alpha)^2$ as a function of photon energy [Figs. 3(c)–3 (f)], where extrapolation of the linear portion of the curve to the x-axis gives the value of the direct band gap.[4]

Figures 3(c)–3(f) shows $(E\alpha)^2$ versus photon energy for (c) Fe_3O_4, (d) Fe_3O_4@$Cu_{2-x}S$, (e) Chlorophyll, and (f) chlorophyllin samples. The direct band gap values are determined by

https://doi.org/10.1557/mrc.2020.39

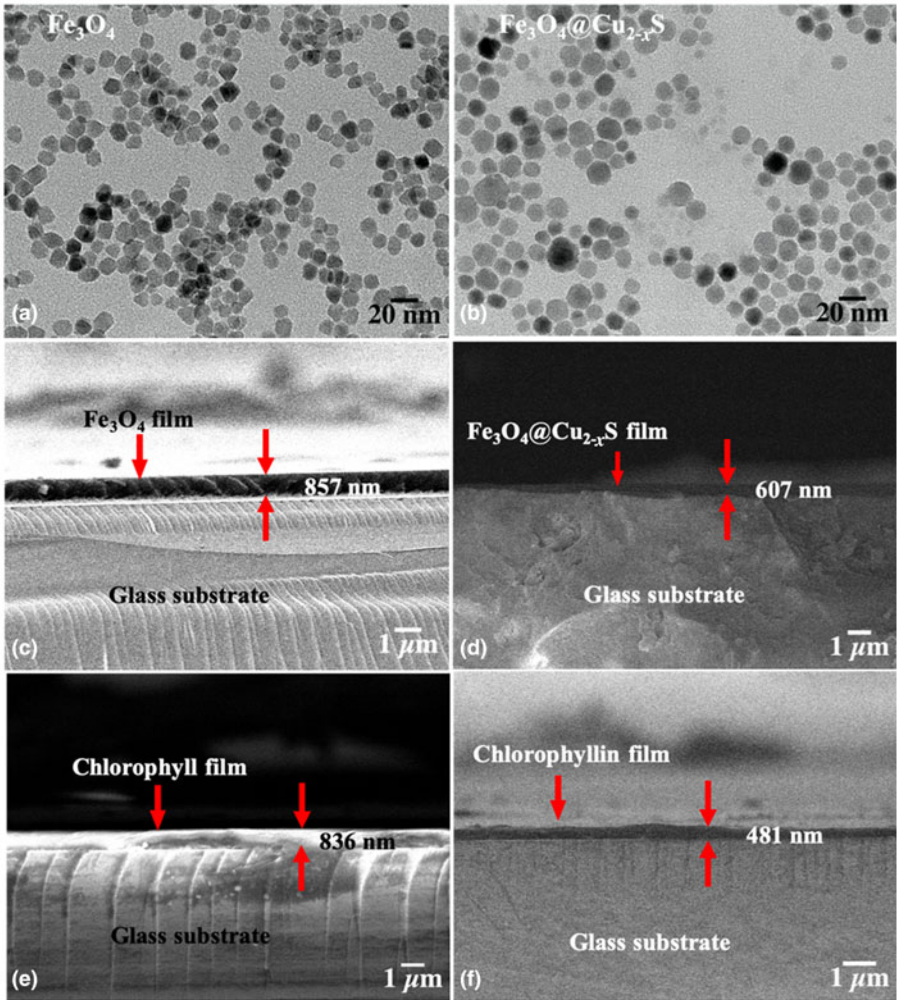

Figure 2. TEM images of (a) Fe_3O_4, (b) $Fe_3O_4@Cu_{2\text{-}x}S$ nanoparticles, and the cross-sectional SEM images of thin film samples, (c) Fe_3O_4, (d) $Fe_3O_4@Cu_{2\text{-}x}S$, (e) chlorophyll, (f) chlorophyllin.

plotting $(E\alpha)^2$ as a function of photon energy. As shown in Figs. 3(c)–3(f), the solid line in each figure represents the experimental absorption curve, and dashed line is the fit to the linear portion of the data, where the intercept of that curve in the x-axis gives the estimation of direct band gap. The band gap energies of Fe_3O_4, $Fe_3O_4@Cu_{2\text{-}x}S$, chlorophyll, and chlorophyllin are, respectively, 3.03 eV, 2.65 eV, 1.81 eV, and 1.82 eV. The band energy of Fe_3O_4 determined in this study (3.03 eV) is consistent with the band gap (~3.1 eV)[8,40,41] between the oxygen orbital (2P) and the photon energy of the octahedral site. The direct band gap of $Fe_3O_4@Cu_{2\text{-}x}S$ (2.65 eV) is lower than that of Fe_3O_4 due to the addition of $Cu_{2\text{-}x}S$ forming a composite core–shell structure.[10] Note that the value of direct band gap of CuS is ~2.2 eV.[42]

The photothermal heating curves were obtained using the experimental set up shown in Fig. 1(d). The distance between the center point of the film sample and the light source was kept the same for measurements at all angles of incidence. In this way, the incident light intensity was maintained at the same level. Figure 4 shows the heating curves for (a) $Fe_3O_4@Cu_{2\text{-}x}S$, (b) Fe_3O_4, (c) chlorophyll, and (d) chlorophyllin samples at concentrations that have resulted in 85% AVT (concentration of each sample: $Fe_3O_4@Cu_{2\text{-}x}S$: 1.1 mg/cm^2, Fe_3O_4: 1.6 mg/cm^2, chlorophyll: 0.9 mg/cm^2, chlorophyllin: 0.7 mg/cm^2). As can be seen in Fig. 4, all samples exhibit clear incident light angle dependence, however, with varied effects. When the angle of incidence is $\theta = 0°$, i.e., the incident light is normal to the film surface, as shown in Fig. 4, all samples reach the highest temperatures of 52.3 °C for $Fe_3O_4@Cu_{2\text{-}x}S$, 47.6 °C for Fe_3O_4, 32.1 °C for chlorophyll, and 34.1 °C for chlorophyllin, respectively. For incident light parallel to the film surface, or $\theta = 90°$, the highest temperatures of the four samples are considerably reduced to 30.5 °C for $Fe_3O_4@Cu_{2\text{-}x}S$, 29.5 °C for Fe_3O_4, 24.2 °C for chlorophyll, and 24.3 °C for chlorophyllin, respectively. Figure 4(e)

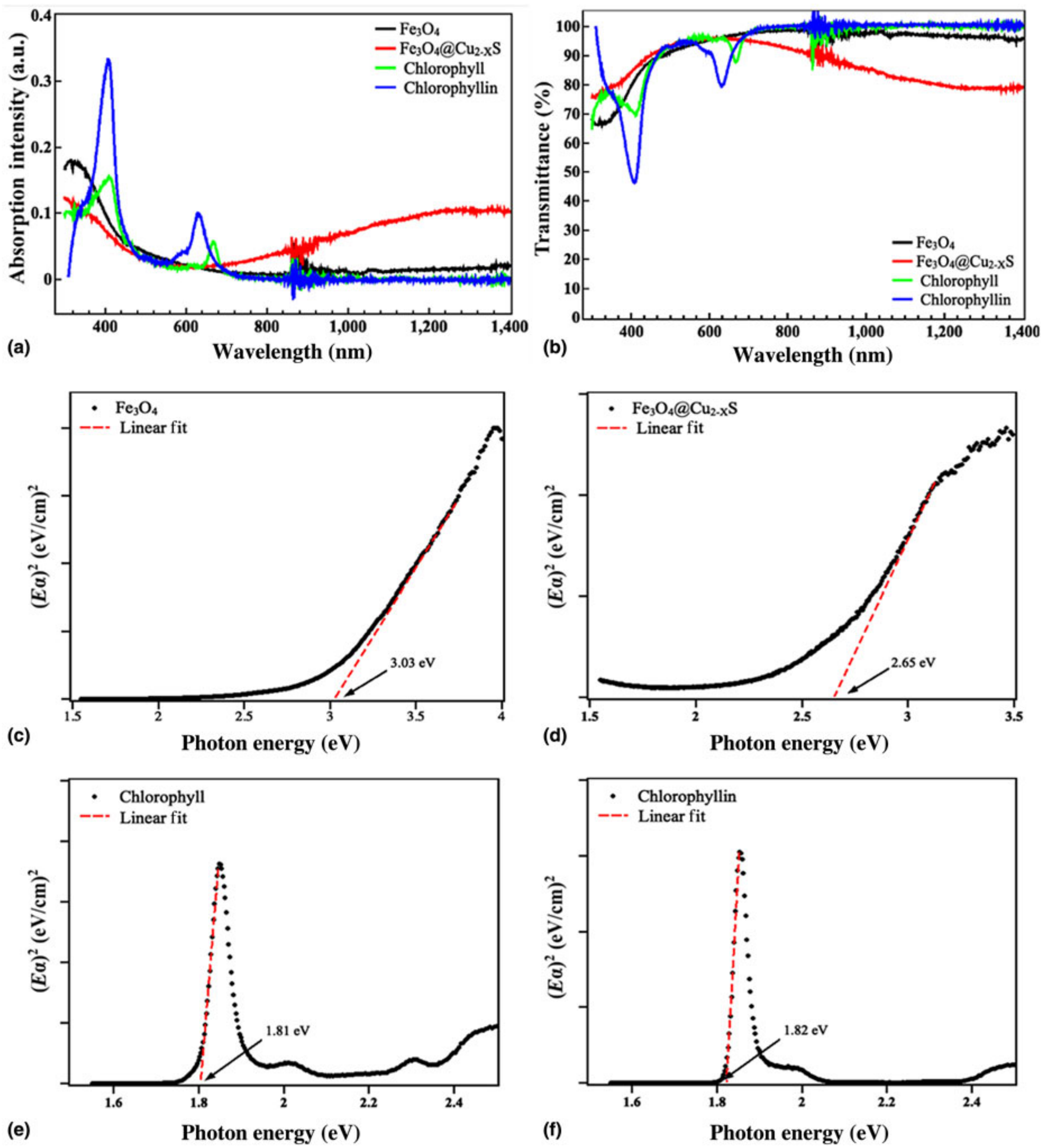

Figure 3. UV analysis of Fe_3O_4, $Fe_3O_4@Cu_{2-x}S$, chlorophyll, and chlorophyllin samples. (a) Absorption, (b) transmittance, and plot of $(E?)^2$ versus photon energy, (c) Fe_3O_4, (d) $Fe_3O_4@Cu_{2-x}S$, (e) chlorophyll, (f) chlorophyllin.

shows the maximum temperature versus angle of incidence for all samples indicated.

The angle dependence of the maximum temperature was found to be associated with the incident light being reflected to a certain degree at varied θ [Fig. 4(f)]. Figure 4(f) shows the light reflected and transmitted for different samples including clear glass and pure PMMA film as controls. As can be seen in this figure, all samples follow the general trends that the light reflectance increases as θ increases. In a reversed manner, transmittance decreases as θ increases. Note that the reflectance and transmittance can only be measured between $\theta = 10°$ and $\theta = 80°$ for placing the light power density meter at the correct position for accurate measurements [Fig. 1(e)].

Discussion

The reflection of light at an interface between different optical media has been well described by the Fresnel equations (or Fresnel coefficients).[43] To simplify the situation, we consider

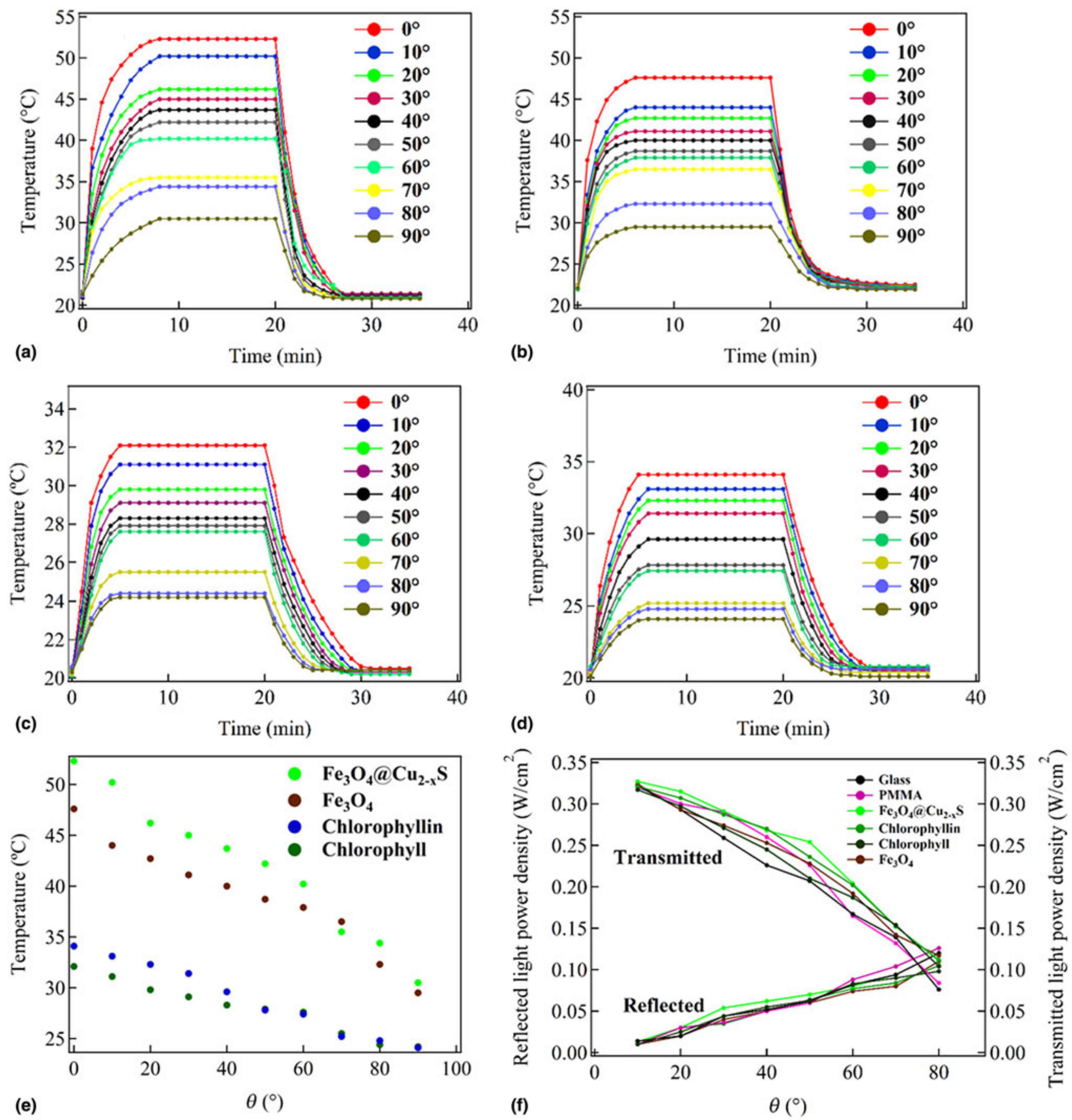

Figure 4. Heating curves of (a) 85% AVT $Fe_3O_4@Cu_{2-x}S$ sample (room temperature 20.9 ± 0.4 °C, humidity 25.6 ± 0.4%), (b) 85% AVT Fe_3O_4 sample (room temperature 22.1 ± 0.4 °C, humidity 27.8 ± 0.3%), (c) 85% AVT chlorophyll sample (room temperature 22.1 ± 0.4 °C, humidity 25.5 ± 0.2%), (d) 85% AVT chlorophyllin sample (room temperature 22.1 ± 0.4 °C, humidity 29.2 ± 0.3%), (e) maximum temperature versus angle of incidence for the samples indicated. All samples are tested with a 0.4 W/cm^2 power density solar simulator of different incident angles from 0° to 90°, (f) reflected and transmitted light power density at different light incident angles.

light propagating in air and striking on an interface which is the boundary of the PT thin film with a greater refractive index (PMMA film containing various PT particles). Since the film is extremely thin (~ 500–800 nm) with a high AVT (85%), we may treat it as an interface between air ($n = 1$) and glass ($n \sim 1.5$). The amount of light reflected at arbitrary incidence angles may follow the law of conservation $R = 1 – T$, where reflectance R = Reflected Power/Incident Power and T is transmittance. The absorbance is negligible due to very thin film and high AVT of the glass substrate. For ideal air/glass interface

https://doi.org/10.1557/mrc.2020.39

(i.e., ideally polished glass surface), Fresnel equations predict that R of unpolarized light is not very angle dependent between 0° and 50° but rapidly increasing above 70°, and approaching one at grazing incidence ($\theta = 90$).[44] However, the reflected light by the PT film steadily increases with the angle of incidence between 10° and 80° almost linearly. Consistently, the transmitted light decreases, for all the PT films studied, with increasing angle of incident.

These data are well correlated to the PT heating curves [Figs. 4(a)–4(d)], particularly with the transmitted light. The photothermal effect accounts for that the amount of light that enters the film, interacting with the electronic and molecular structures of the PT materials, and consequently converting photons to thermal energy resulting in the temperature increase. The light that is reflected does not contribute to the photothermal effect. The difference between the experimental data shown in Fig. 4(f) and the Fresnel curves[43] can be attributed to the non-ideal surfaces of the thin film. Significant light scattering takes place on the non-ideal and rough film surfaces (diffuse reflection) causing significantly reduced light to be reflected particularly at a high angle of incidence.[45–48]

Furthermore, light is, in fact, reflected at two surfaces, one from the film top, and the other from the bottom of the thin film. Part of the light reflected from the bottom surface can interfere with light reflected from the top, both may be in or out of phase depending on the thickness of the film which has a greater refractive index than that of air.[47] PMMA has a refractive index of 1.4905 at 589.3 nm and visible transmittance of 92%. For very thin films (in this study, the thickness is 500–800 nm), the difference in path lengths of light reflected by both surfaces is negligible. However, there is a phase change when light travels through the film. Under white light irradiation, constructive interference occurs as the thickness varies. While the reflected light rays at both surfaces contribute to total reflectance, portions of them are also responsible for the photothermal effects as light travels through the film and internally reflected multiple times. Further studies will focus on modeling of light reflection, refraction, and transmittance of the thin film that can be correlated to the experimental heating curves.

As illustrated in Fig. 1, the sunlight incident angle, $\alpha = \theta$ (the photothermal experimental angle of incidence). According to the results on the angle (α) dependence of the photothermal effect (Fig. 4), one can see the highest temperatures reached when light is normal to the plane of interface ($\theta = 0°$). At the winter solstice in Chicago, $\alpha = \theta = 24.70°$. From the heating curves in Fig. 4, we can see the maximum temperatures reached by the PT films at 20°: $Fe_3O_4@Cu_{2-x}S$: 46.2 °C; Fe_3O_4: 42.7 °C; chlorophyll: 29.8 °C, and chlorophyllin: 32.3 °C. The ΔT gained via photothermal thin film coatings will significantly reduce the thermal loss through the single pane. It should be noted that these temperature increases are achieved by extremely thin films (~500–800 nm). As the photothermal effect is an extensive property, thicker films will substantially increase the surface temperature, and further reducing the U-factor.

At the summer solstice, $\alpha = \theta = 71.70°$. From Fig. 4, we find temperatures reached by the PT films at 70°: $Fe_3O_4@Cu_{2-x}S$: 35.5 °C; Fe_3O_4: 36.5 °C; chlorophyll: 25.5 °C, and chlorophyllin: 25.2 °C, all are considerably lower compared to those obtained at 20° (winter solstice). Therefore, in the summer season at solar noon, considerable incoming sunlight is not directly striking on the window glass and the photothermal effect would be weakened. At winter solstice, the window surfaces receive most of the sunlight for the highly enhanced photothermal effect and window surface temperature will therefore increase, significantly reducing the heat loss in cold weather. The results on the incident sunlight angle dependence (Fig. 4) show the seasonal and daily factors that may influence the photothermal effect, resulting from the PT thin film coatings on the window glasses. It is an experimental proof of the optical thermal insulation (OTI) that the photothermal coating on the window surface is an effective and viable way of achieving thermal insulation without any conventional intervention medium and the glazing technologies can be straightforwardly simplified.

Conclusion

The thin films of Fe_3O_4, $Fe_3O_4@Cu_{2-x}S$, chlorophyll, and chlorophyllin were deposited on glass substrates by spin coating and well characterized on both microstructural and optical properties. These thin films exhibited uniform microstructures (Fig. 2) with thicknesses in the range of ~ 500–800 nm. Due to extremely thin films, high visible transmittances above 90% were achieved for all photothermal materials studied in wide spectra (Fig. 3). Both chlorophyll and chlorophyllin thin films were characterized with absorption peaks near the UV and NIR regions, particularly useful not only for efficient solar light harvesting but enhanced transparency (Fig. 3). It was also found that, compared to Fe_3O_4, $Fe_3O_4@Cu_{2-x}S$ exhibited pronounced NIR absorption in a broad range which largely contributes to increased photothermal effect (Fig. 4).

The incident light angle dependence of the photothermal effect experiments was performed using the simulated solar light with 0.4 W/cm^2. The angle of incidence was varied from 0° to 90° in order to observe its effects on the heating curves (Fig. 4). Considerable angle dependence was observed with the highest temperature reached for 0° and lowest temperature at 90°. This angle dependence was found to be directly associated with the light being reflected by the thin film surfaces, however, in a more gradual fashion compared to the ideal interface as described by the Fresnel equations. The reduced light reflection, particularly near grazing incidence ($\theta = 90°$), is explained by light scattering on non-ideal surfaces of the as-deposited thin films, although rather uniform from a processing point of view. The light transmitted through the thin film in fact contributes to the temperature rise via the photon interactions with the electronic structure of Fe_3O_4, $Fe_3O_4@Cu_{2-x}S$[10], and molecular structure of chlorophyll[9] and chlorophyllin.[15] While the photothermal mechanism of iron-oxide based materials has been identified as the localized plasmonic surface resonance (LPSR)[10], the photon-to-heat conversion attributes to the molecular vibrations in the porphyrin structures of chlorophyll and chlorophyllin.[15]

The U-factors of Fe_3O_4, $Fe_3O_4@Cu_{2-x}S$, and chlorophyll have been calculated by using the National Fenestration Rating Council (NFRC) standardized equation in a previous work.[13] These U-factor values have been shown to meet the requirement of Energy Star certification that $U < 1.7$ W/m^2 K.[14] These results also indicate that thermal transmittance (U-factor) can be reduced by applying photothermal coatings on single-pane window surfaces[8,9], achieving the optical thermal insulation without any intervening gas media in conventional glazing technologies.

It is concluded that the photothermal effect of a two-dimensional thin film exhibits an incident light angle dependence, which is mainly associated with the light reflected by and transmitted through the film interfaces. However, the heat generated by the thin film can be affected by other factors such as refractive indices, constructive or destructive interferences, film thickness, and the wavelength of the incident light, be it monochromatic or white. It is also concluded that, for window designs to reduce the thermal energy loss especially for cold climates, optical thermal insulation via the photothermal thin film coating is viable and straightforward in materials synthesis, architectural designs, and civil engineering applications.

Acknowledgments

This research is supported by National Science Foundation CMMI-1635089. We would like to thank Dr. Andrew J. Steckl for the Perkin-Elmer spectrophotometer.

References

1. EIA: *Consumption & Efficiency*. U.S. Energy Information Administration (2015). https://www.eia.gov/consumption/ (accessed March 10, 2020).
2. A.A.F. Husain, W.Z.W. Hasan, S. Shafie, M.N. Hamidon, and S.S. Pandey: A review of transparent solar photovoltaic technologies. *Renew. Sust. Energy Rev.* **94**, 779–791 (2018).
3. S.Y. Chang, P. Cheng, G. Li, and Y. Yang: Transparent polymer photovoltaics for solar energy harvesting and beyond. *Joule* **2**, 1039–1054 (2018).
4. D. Shi, M.E. Sadat, A.W. Dunn, and D.B. Mast: Photo-fluorescent and magnetic properties of iron oxide nanoparticles for biomedical applications. *Nanoscale* **7**, 8209–8232 (2015).
5. I. Sartori, A. Napolitano, and K. Voss: Net zero energy buildings: a consistent definition framework. *Energy Build.* **48**, 220–232 (2012).
6. L. Wang, J. Gwilliam, and P. Jones: Case study of zero energy house design in UK. *Energy Build* **41**, 1215–1222 (2009).
7. S. Attia, E. Gratia, A. De Herde, and J.L.M. Hensen: Simulation-based decision support tool for early stages of zero-energy building design. *Energy Build* **49**, 2–15 (2012).
8. Y. Zhao, M.E. Sadat, A. Dunn, H. Xu, C.H. Chen, W. Nakasuga, R.C. Ewing, and D. Shi: Photothermal effect on Fe_3O_4 nanoparticles irradiated by white-light for energy-efficient window applications. *Sol. Energy Mater. Sol. Cells* **161**, 247–254 (2017).
9. Y. Zhao, A.W. Dunn, and D. Shi: Effective reduction of building heat loss without insulation materials via the photothermal effect of a chlorophyll thin film coated Green Window. *MRS Commun.* **9**, 675–681 (2019).
10. J. Lin, Y. Zhao, and D. Shi: Optical thermal insulation via the photothermal effects of Fe_3O_4 and $Fe_3O_4@Cu_{2-x}S$ thin films for energy-efficient single-pane windows. *MRS Commun.* **10**, 155–163 (2020).
11. J. Wang and D. Shi: Spectral selective and photothermal nano structured thin films for energy efficient windows. *Appl. Energy* **208**, 83–96 (2017).
12. J.S. Choi, B.G. Choi, J.H. Kim, S.T. Ryu, C.T. Rim, and Y.S. Kim: New curved reflectors for significantly enhanced solar power generation in four seasons. *Energies* **12**, 4602 (2019).
13. National Fenestration Rating Council: *Procedure for Determining Fenestration Product U-factors* (2013). https://www.nfrccommunity.org/store/ViewProduct.aspx?id=1380591 (accessed March 10, 2020).
14. E. Energy Star: *ENERGY STAR Program Requirements for Residential Windows, Doors, and Skylights*. https://www.energystar.gov/sites/default/files/Windows_Doors_and_Skylights_Program_Requirements%20v6.pdf (accessed March 12, 2020).
15. Y. Zhao, J. Lin, D.M. Kundrat, M. Bonmarin, J. Krupczak Jr., S.V. Thomas, M. Lyu, and D. Shi: Photonically-activated molecular excitations for thermal energy conversion in porphyrinic compounds. *J. Phys. Chem. C* **124**, 1575–1584 (2020).
16. Solar Energy: http://www.inforse.org/europe/dieret/Solar/solar.html (accessed March 13, 2020).
17. Working with Solar Fabircs: https://ecofabrix.com/fabric-guide/ (accessed March 07, 2020).
18. Y.M. Chen, C.H. Lee, and H.C. Wu: Calculation of the optimum installation angle for fixed solar-cell panels based on the genetic algorithm and the simulated-annealing method. *IEEE Trans. Energy Convers* **20**, 467–473 (2005).
19. M. Born, E. Wolf, A.B. Bhatia, P.C. Clemmow, D. Gabor, A.R. Stokes, A.M. Tayler, P.A. Wayman, and W.L. Wilcock: *Principles of Optics*. 7th ed. (Cambridge University Press, England, 1999).
20. The Carbon Neutral Design Project, Society of Building Science Educators, American Institute of Architects: *Carbon Neutral Design Strategies* (2012). http://www.tboake.com/carbon-aia/strategies1a.html (accessed March 11, 2020).
21. Solar Geometry: http://mypages.iit.edu/~maslanka/SolarGeo.pdf (accessed March 13).
22. W.B. Stine and M. Geyer: *Power from the Sun* (eBook, 2001). http://www.powerfromthesun.net/book.html (accessed March 11, 2020).
23. A. El-Sebaii and A.E.M. Khallaf: Mathematical modeling and experimental validation for square pyramid solar still. *Environ. Sci. Pollut. Res.* Published online 11 Jan 2020. doi:10.1007/s11356-019-07587-5
24. M. Khan: Solar still distillate productivity enhancement by using reflector and design optimization experimental investigation of nucleate pool boiling heat transfer enhancement of TiO_2-water based nanofluids view project. *Innov. Ener. Res.* **8**, 222 (2019).
25. M.J. Yun, Y.H. Sim, S.I. Cha, S.H. Seo, and D.Y. Lee: 3-Dimensional dye sensitized solar cell sub-module with oblique angled cell array for enhanced power and energy density output utilizing non-linear relation in cosine law of light incident angle. *Sol. Energy* **177**, 355–363 (2019).
26. Y.Q. Liu, D. Wei, H.L. Cui, and D.Q. Wang: Photovoltaic effect related to methylammonium cation orientation and carrier transport properties in high-performance perovskite solar cells. *ACS Appl. Mater. Interfaces* **12**, 3563–3571 (2020).
27. J.X. Liu, Q. Tian, J. Hu, Y. Zhu, R. Zou, and Z. Chen: Sub-10 nm $Fe_3O_4@Cu_{2-x}S$ core-shell nanoparticles for dual-modal imaging and photothermal therapy. *J. Am. Chem. Soc.* **135**, 8571–8577 (2013).
28. S. Upadhyay, K. Parekh, and B. Pandey: Influence of crystallite size on the magnetic properties of Fe_3O_4 nanoparticles. *J. Alloys Compd.* **678**, 478–485 (2016).
29. S. Ali, S.A. Khan, J. Eastoe, S.R. Hussaini, M.A. Morsy, and Z.H. Yamani: Synthesis, characterization, and relaxometry studies of hydrophilic and hydrophobic superparamagnetic Fe_3O_4 nanoparticles for oil reservoir applications. *Colloids Surfaces A Physicochem. Eng. Asp* **543**, 133–143 (2018).
30. K. Nee Koo, A. Fauzi Ismail, M. Hafiz Dzarfan Othman, M.A. Rahman, and T. Zhong Sheng: Preparation and characterization of superparamagnetic magnetite (Fe_3O_4) nanoparticles: a short review. *Malays. J. Fundam. Appl. Sci.* **15**, 23–31 (2019).
31. A. Nagaraja, Y.M. Puttaiahgowda, A. Kulal, A.M. Parambil, and T. Varadavenkatesan: Synthesis, characterization, and fabrication of hydrophilic antimicrobial polymer thin film coatings. *Macromol. Res.* **27**, 301–309 (2019).

32. W.R. Wu, C.J. Su, W.T. Chuang, Y.C. Huang, P.W. Yang, P.C. Lin, C.Y. Chen, T.Y. Yang, A.C. Su, K.H. Wei, C.M. Liu, and U.S. Jeng: Surface layering and supersaturation for top-down nanostructural development during spin coating of polymer/fullerene thin films. *Adv. Energy Mater.* **7**, 1601842 (2017).
33. S. Wang, X. Zhao, Y. Tong, Q. Tang, and Y. Liu: Directly spin coating a low-viscosity organic semiconductor solution onto hydrophobic surfaces: toward high-performance solution-processable organic transistors. *Adv. Mater. Interfaces* **7**, 1901950 (2020).
34. M.V. Kelso, N.K. Mahenderkar, Q. Chen, J.Z. Tubbesing, and J.A. Switzer: Spin coating epitaxial films. *Science* **364**, 166–169 (2019).
35. H. Inoue, H. Yamashita, K. Furuya, Y. Nonomura, N. Yoshioka, and S. Lib: Determination of copper(II) chlorophyllin by reversed-phase high-performance liquid chromatography. *J. Chromatogr. A* **679**, 99–104 (1994).
36. E. Yuliarita and A. Zulys: Utilization of natural compounds (chlorophyll and carotene extracts) as an octane-boosting additive in gasoline. *IOP Conf. Ser. Mater. Sci. Eng.* **496**, 012048 (2019).
37. B. Zhang, Y. Shan, and K. Chen: A facile approach to fabricate of photo-thermal functional Fe_3O_4@CuS microspheres. *Mater. Chem. Phys.* **193**, 82–88 (2017).
38. J. Singh: *Optical Properties of Condensed Matter and Applications* (Wiley, Chichester, UK, 2006).
39. R.C. Rai: Analysis of the Urbach tails in absorption spectra of undoped ZnO thin films. *J. Appl. Phys.* **113**, 153508 (2013).
40. C. Boxall, G. Kelsall, and Z. Zhang: Photoelectrophoresis of colloidal iron oxides: Part 2. - Magnetite (Fe_3O_4). *J. Chem. Soc. - Faraday Trans.* **92**, 791–802 (1996).
41. W.F.J. Fontijn, P.J. van der Zaag, L.F. Feiner, R. Metselaar, and M.A.C. Devillers: A consistent interpretation of the magneto-optical spectra of spinel type ferrites. *J. Appl. Phys.* **85**, 5100–5105 (1999).
42. K.R. Nemade, and S.A. Waghuley: Band gap engineering of CuS nanoparticles for artificial photosynthesis. *Mater. Sci. Semicond. Process* **39**, 781–785 (2015).
43. D. Miyazaki: Fresnel Equations (2014). https://link.springer.com/content/pdf/10.1007%2F978-0-387-31439-6_569.pdf (accessed March 11).
44. E. Hecht: *Optics*. 3rd ed. (Addison-Wesley Longman, Inc., Boston, MA, 1998).
45. A.A. Maradudin and E.R. Méndez: Light scattering from randomly rough surfaces. *Sci. Prog.* **90**, 161–221 (2007).
46. D. Nolan, W. Senaratne, D. Baker, and L. Liu: Optical Scattering from Nanostructured Glass Surfaces. *Int. J. Appl. Glas. Sci.* **6**, 345–355 (2015).
47. D.G. Stavenga: Thin film and multilayer optics cause structural colors of many insects and birds. *Mater. Today: Proc.* **1**, 109–121 (2014).
48. G.A. Atkinson and E.R. Hancock: Shape estimation using polarization and shading from two views. In *IEEE Transactions on Pattern Analysis and Machine Intelligence* (IEEE, **29**, Piscataway, New Jersey, US, 2007), pp. 2001–2017.